Proceedings Paper:
Hara, YRS and Jha, A orcid.org/0000-0003-3150-5645 (2015) Energy efficient separation of magnetic alloy from the carbothermic reduction of NKANA Cu-Co concentrates. In: Jha, A, Wang, C, Neelameggham, NR, Guillen, DP, Li, L, Belt, CK, Kirchain, R, Spangenburger, JS, Johnson, F, Gomes, AJ, Pandey, A and Hosemann, P, (eds.) Energy Technology 2015: Carbon Dioxide Management and Other Technologies. TMS 2015 144th Annual Meeting & Exhibition, 15-19 Mar 2015, Orlando, Fla., U.S.A.. Springer , pp. 83-92. ISBN 978-3-319-48602-4

https://doi.org/10.1007/978-3-319-48220-0_10

Thermodynamic and kinetic analysis of low temperature ($T \leq 1323$ K) recovery of Cu, Co and Fe from SiO_2-CaO-$(Al, Fe)_2O_3$ Slag

Yotamu R.S. Hara and Animesh Jha

The Institute for Materials Research, Houldsworth Building
Clarendon Road, Leeds University, Leeds, LS2 9JT (UK), England

Abstract

The investigation focuses on direct reduction and sulphidization of Cu-Co slag via equations; MO + C = M + CO(g) and MO + $CaSO_4$ + 4C = MS + CaO + 4CO, respectively, where M represents metallic Cu, Co and Fe, over a temperature range of 1173 K – 1323 K. The expriments were carried out in the thermogravimetric analysis (TGA) equipment and the reacted samples were characterized by X-ray diffraction (XRD) and scanning electron microscopy (SEM) techniques. The direct reduction was sensitive to the reaction temperature and type of carbon and, the highest reduction was about 90 % at 1323 K, with activated charcoal. The reaction kinetics for the direct reduction of slag was analysed; the experimental data fitted into the mixed reaction model and the activation energy was 160 kJ – 290 kJ. The metal oxides in slag were transformed to metal sulphides ($CuFeS_2$, FeS, $Co_xFe_{1-X}S$, Cu_5FeS_4 etc) when slag was sulphidized in the presence of $CaSO_4$ and graphite. The effect of reaction temperature and molar ratio of graphite was studied and high sulphidization was obtained at $T \geq 1273$ K and molar ratio of MO:$CaSO_4$:C = 1:1.3:1.5. The overall sulphidization of slag was limited by the CO_2 – C reaction at $T < 1273$ K with activation energy of 311 ± 6 kJ. The sulphidized slag was reduced in the presence of CaO and C via MS + CaO + C = M + CaS + CO(g) reaction and, metallization was completed within 1.5 hours at 1173 K. The metallic/alloy particles produced via sulphidization – carbothermic reduction route were larger than those produced via direct reduction.

Key words: matte, metal sulphides, slag, reaction kinetics, Co alloy, carbothermic reduction

1.0 Introduction

Copper and cobalt are the two main valuable components in the conventional copper smelting slag [1-3]. These metals enter the slag phase via: (i) oxidation [2] and (ii) entrapment of metallic (Cu and Co) and metal sulphides (Cu_2S, Cu_5FeS_4 and CoS) [2]. By comparison, a majority of Co and Cu in slag are in the form of oxide and sulphide state, respectively [1]. Mineralogical studies have showed that the metal oxides (Cu_2O, CuO and CoO) are mainly dissolved in fayalite (Fe_2SiO_4), magnetite (Fe_3O_4) and glassy phases [1, 4]. The copper smelting slag dump may contain up to 2 wt. % Cu [4] and 0.8 wt.% Co [1]. According to London Metal Exchange, the current price (November, 2014) of copper and cobalt per tonne of metal is about $7000 and $31500, respectively. Comparing the composition of Cu and Co in slag and in mineral concentrates, the slag becomes an important source of these metals.

1.1 Hydrometallurgical recovery of Cu and Co from slag

Leaching – electro-winning is the common method by which Cu and Co are recovered from the oxide minerals [2]. However, the oxides of Cu and Co in slag are dissolved in silicate and ferrite phases and, leaching of these phases yields silica gel and increased concentration of iron in leach solution, respectively. The formation of silica gel makes filtration extremely difficult. Overcoming these two problems remains a challenging in the hydrometallurgical recovery of Cu and Co from slag, which would otherwise be the easiest route.

1.2 Pyro – hydro metallurgical processing of slag

In pyro – hydro metallurgical process, Cu-Co slag is roasted with pyrite (FeS_2) [5, 6], sulphuric acid (H_2SO_4) [3], ferric sulphate ($Fe_2(SO_4)_2$) [7] or ammonium sulphate ($(NH_4)_2SO_4$) [8] to yield Cu and Co sulphates. The roasted slag is leached in water or acid to selectively dissolve Cu and Co sulphates. The leach solution is purified to remove impurities and, Cu and Co are recovered from the leach solution via electro-winning process. However, the recovery of Co is low via this method [6, 7].

1.3 Pyrometallurgical processing of slag

1.3.1 Carbothermic reduction of slag

In carbothermic reduction, the metal oxides are reduced by carbon according to equation 1 [9]. However, the metal sulphides (Cu_2S, Cu_5FeS_4, $CuFeS_2$) [2] in the slag cannot be reduced by carbon. The carbothermic reduction may be good for: (i) recovering Co from slag as it is mainly in the oxide form and, (ii) production of Cu-Co rich matte ($Co{\cdot}Cu{\cdot}Cu_2S{\cdot}Cu_5FeS_4$).

$$MO + C = M + CO(g) \quad (1)$$

Where MO and M represents metal oxide and metallic phase, respectively.

Nearly all Fe is reduced and, a molten Fe rich Cu-Co-Fe alloy and slag are produced at high temperature (> 1823 K) [1, 10-14]. The Fe rich Cu-Co-Fe alloy is atomized, leached in autoclave and, Cu and Co are recovered from the solution via electro-winning.

1.3.2 Sulphidization of slag

Sulphidization is the conversion of metal oxides (Cu_2O, CoO, FeO etc.) or metallic (Co, Co and Fe) into metal sulphides (Cu_2S, CoS, FeS etc.). The main advantage of this process is that metallic, metal oxides and metal sulphides are recovered as metal sulphides or matte phase. Sulphidization of slag in the presence of $CaSO_4$ and C may involve the following steps: (i) reduction calcination of $CaSO_4$ gas (equation 2) and, (ii) reaction between SO_2 gas and metal oxide (MO) (equation 3). The summation of equations 2 and 3 gives equation 4. The use of very reactive carbon or higher molar ratio of C may decrease sulphidization due to formation of CaS via reaction 5 [15].

$$CaSO_4 + 0.5C = CaO + SO_2 + 0.5CO_2(g) \quad (2)$$

$$MO + SO_2(g) + 1.5C = MS + 1.5CO_2(g) \quad (3)$$

$$MO + CaSO_4 + 2C = MS + CaO + 2CO_2(g) \quad (4)$$

$$CaSO_4 + 2C = CaS + 2CO_2(g) \quad (5)$$

The advantages of sulphidizing slag in the presence of $CaSO_4$ are:

i. $CaSO_4$ is readily available as it is a waste product from the thermal power plants [16] and from Cu-Co leach plant [3].
ii. Sulphidization may be achieved with minimal or no generation of SO_2 gas, unlike in the presence of pyrite (FeS_2) where part of S_2/SO_2 gases escape, owing to the rapid decomposition of FeS_2 above 1016 K.
iii. Calcium silicate rich slag may be produced which may be used for construction and glass making.

The sulphidization of Cu-Co slag in the presence of $CaSO_4$, has been studied by Matusewicz and Mounsey [5] and it was reported that $CaSO_4$ is inappropriate for facilitating matte production [5]. However, no details were given out as regards to reaction temperature, type of carbon and stoichiometric ratios of $CaSO_4$ and carbon.

The Cu-Co-Fe-Ca-Si-O-S predominance area diagram at 1273 K is shown in figure 1 from which it can be observed that complete sulphidization is possible as metal sulphides ($CuFeS_2$, Cu_5FeS_4, Co_9S_8, FeS) co-exist with $CaSiO_3$ and SiO_2 at $\log_{10}(P(O_2)) < -10$. It can further be observed in figure 1 that metal oxides ($CoFe_2O_4$ and Cu_2O) co-exist with $CaSO_4$, $CaSiO_3$ and SiO_2 at $\log_{10}(P(O_2)) > -6.4$ which means that sulphidization may not be achieved at high partial pressure of O_2 gas. It is evident from the thermodynamic prediction in figure 1 that Cu_2S/Cu_5FeS_4 or $Cu_2S + Co_9S_8$ may be formed preferentially by controlling the partial pressure of O_2 gas and this is good for the selective sulphidization of Cu and Co from slag.

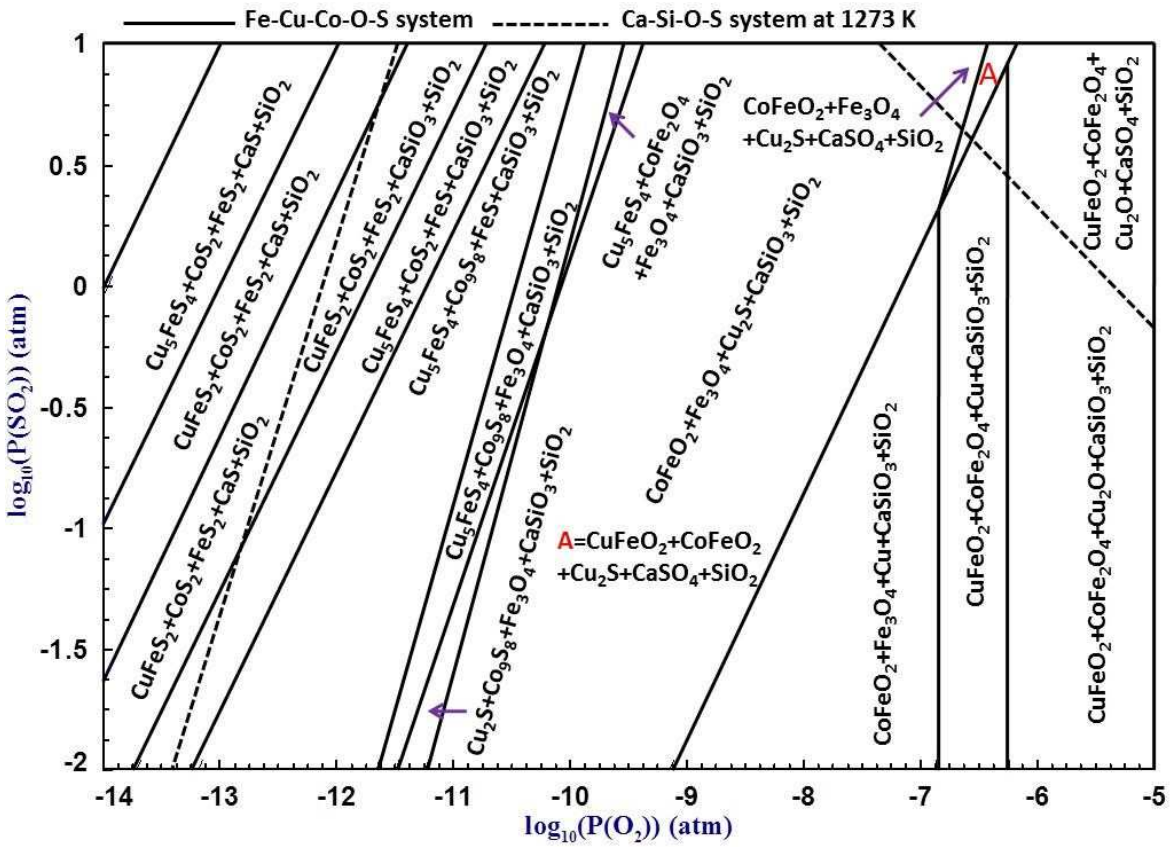

Figure 1 – Computed Fe-Co-Fe-Ca-Si-O-S predominance area diagram at 1273 K, Fe-Co-Fe-O-S (continuous line) and Ca-Si-O-S (dotted line), using FactSage software [17]

As shown from the thermodynamic prediction in figure 1, Cu, Co and Fe sulphides (matte) may be produced via sulphidization of the slag at 1273 K. The sulphidized slag may be treated through a number of processes to recover Cu and Co:

i. Carbothermic reduction of sulphidized slag in the presence of CaO (equation 6) and magnetic separation may yield metallic (Cu, Co and Fe) and non-magnetic fraction containing CaS and $CaSiO_3$. CaS may be oxidised to $CaSO_4$ (equation 7) and recycled into the process.

$$MS + CaO + C = M + CaS + CO(g) \qquad 6$$

$$CaS + 2O_2(g) = CaSO_4 \qquad 7$$

ii. Holding the sulphidized slag at about 1523 K in order to allow matte / slag phase separation. The matte phase may be processed as Cu-Co sulphide concentrates.

iii. Froth flotation of the metal sulphides [2].

2.0 Experimental

2.1 Materials

The Cu-Co slag was synthesized in the laboratory by melting the mixture of metal oxides (CuO, CoO, Fe_2O_3), Al_2O_3, CaO and SiO_2 according to table 1. The composition in table 1 is typical of Nkana copper smelting slag [18] except that CuO and CoO were added in higher quantities for easy analysis and understanding of metal recovery. For synthesis, the sample was melted in air, for 2 hours at 1523 K. The sample was taken out of the furnace when it had cooled down to 1323 K. The cooled slag sample was crushed and ground to –200 µm particle size.

Table 1 – Composition of the synthetic slag in wt.%

Constituent	SiO_2	CaO	Fe_2O_3	Al_2O_3	CoO	CuO
Weight (%)	40	10	30	6	7	7

Carbon black was supplied by Evonik Company (Germany) and activated charcoal was purchased from ACROS, both had particle size of less than 50 µm. Anhydrous calcium sulphate ($CaSO_4$) and calcium oxide (CaO) with purities of > 99 % were purchased from Alfar Aesar (UK).

2.2 Reduction and sulphidization experiments

Carbothermic reduction – 1.4 g of slag was mixed thoroughly with carbon (carbon black and activated charcoal) at three times the stoichiometric ratio (MO:C = 1:3).
Sulphidization of slag – 1.2 g of slag was mixed with $CaSO_4$ and C (graphite) by following the stoichiometric conditions in equation 4.

The carbothermic reduction and sulphidization experiments were carried out isothermally, in the thermogravimetric analysis (TGA) equipment, in order to study the weight loss as a function of time. Details of the thermogravimetric analysis equipment are found in

our previous studies [19, 20]. The reaction chamber was purged with argon gas at a flow rate of 0.6 litre min^{-1}, for maintaining inert atmosphere [19]. The weight loss of the sample was recorded at an interval of 10 seconds, throughout the experiments. The % reduction or the % CO gas given out at any time for the carbothermic reduction of slag was calculated from equation 8.

$$\%reduction\ \ at\ any\ time = \frac{\exp erimental\ \ weight\ \ loss\ at\ any\ time}{T_{Wt}CO} \times 100\% \qquad 8$$

Where $T_{wt}CO$ is the theoretical weight loss of CO gas from equation 1

The % conversion or % sulphidization of slag in the presence of $CaSO_4$ and graphite was calculated according to equation 9.

$$\%conversion\ at\ any\ time = \frac{\exp erimental\ \ weight\ \ loss\ at\ any\ time}{T_{wt}CO_2} \times 100\% \qquad 9$$

Where $T_{wt}CO_2$ is the theoretical weight loss of CO_2 gas from equation 4

2.3 Characterisation of the samples

The samples were characterised by X-ray diffraction (XRD) and scanning electron microscopy (SEM) techniques.

X-ray powder diffraction analysis: A representative portion of the sample was ground, packed into the sample holder and analysed by the Philips X'pert machine with a copper Kα radiation (λ = 1.5417 Å). The machine was operated at 40 kV, 30 mA and step size of 2θ = 0.03315 º. The phases in the powder diffraction patterns were analysed by the X'pert high score plus software which is supported by the JCPDS PDF-4+ data base (RDB 2013) [20].

Scanning electron microscopy (SEM): The sample was mounted in a mixture of 3 parts epoxy hardener and 1 part epoxy hardener and, cured for 8 hours. After the resin had set, the samples were released from the moulds and gently ground on different grades of silicon carbide paper. The samples were placed inside the Agar high resolution sputter coater and coated with a 6 nm thick layer of platinum, to minimise charging during SEM imaging. The samples were

examined for structural and chemical changes over a large area in order to understand the distribution of the phases.

3.0 Results and discussion

Synthetic slag was analysed by X-ray powder diffraction (XRD) and scanning electron microscopy (SEM) techniques and the results are presented in figures 2 and 3, respectively. It is evident from the XRD pattern in figure 2 that $Co_{0.62}Fe_{2.38}O_4$ and SiO_2 are the only crystalline phases. Ca and Al are in the amorphous glassy phase [21] and the presence of amorphous phase is evident as there is a broad peak for 2θ between 20º and 34º [22]. The SEM images in figures 3a and 3b confirms that there is an amorphous and two crystalline phases. SEM-EDX semi-quantitative composition of the phases in figures 3a and 3b are presented in table 2 from which it can be observed that the $Co_{0.68}Fe_{2.38}O_4$ crystals contains up to 7 wt. % Cu. The $Co_{0.62}Fe_{2.38}O_4$ phase occurs as smaller euhedral to subheudral crystals and this texture suggests that this phase crystallised earlier during slow cooling of the melt [21, 23, 24]. The glassy phase should contain mainly Si, Ca and Al [21] but it has all elements Si, Ca, Cu, Fe, Al and Co in the decreasing order since it hosts the elements that fail to enter or form crystalline phases [21, 24].

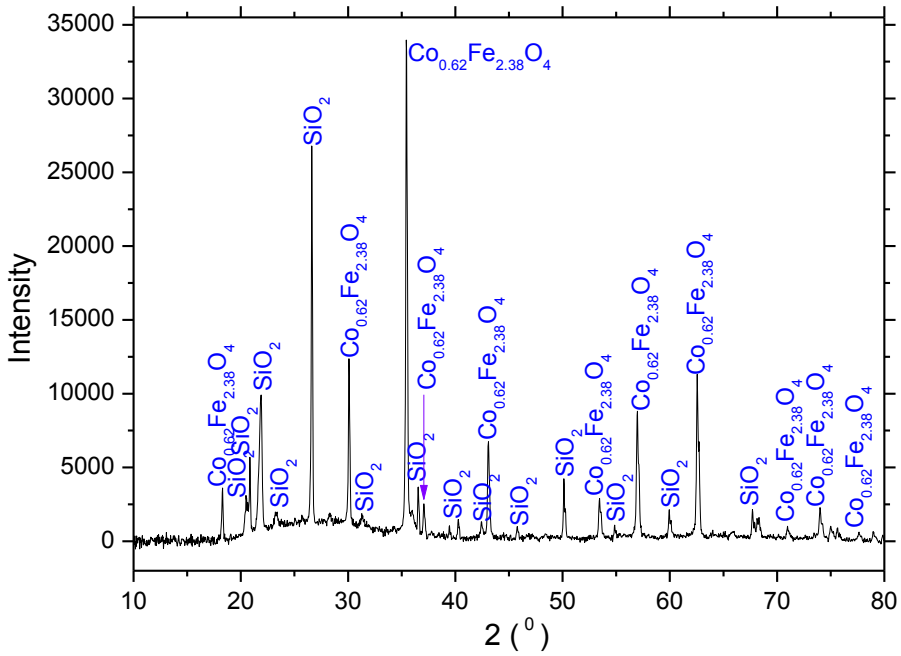

Figure 2 – XRD pattern for the slag, synthesised in air for 2 hours at 1523 K

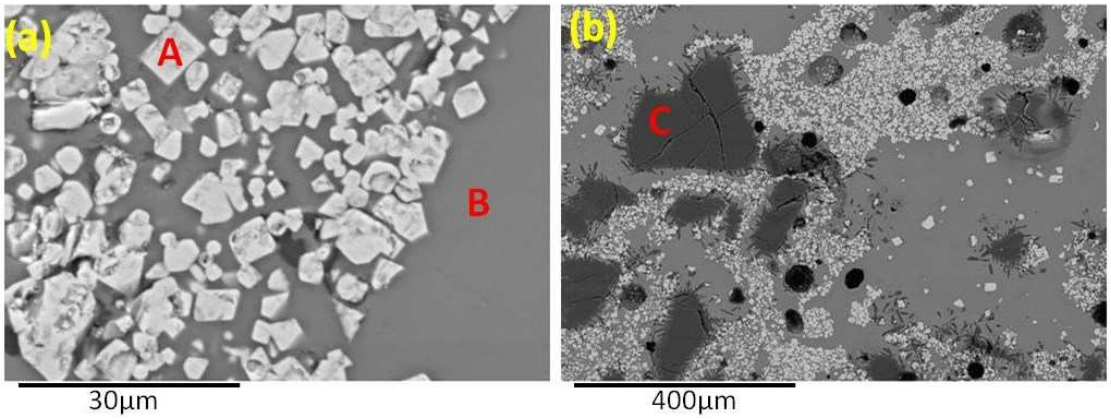

Figure 3 – Backscattered SEM images of the slag, synthesised in air for 2 hours at 1523 K, the composition of areas A, B and C are presented in table 2

Table 2 - EDX semi-quantitative analysis (wt. %) of areas A, B and C from figures 3a and 3b

Area	Cu	Fe	Co	Si	Ca	Al	O
A	3.6	52.8	13.8	-	-	0.8	28.7
B	10.3	6.4	1.9	23.1	11.6	4.2	42.5
C	-	-	-	46.4	-	-	53.6

3.1 Carbothermic reduction of slag

It was important to investigate low temperature reduction because most of Co in slag dumps is in the oxide form [1]. Furthermore, the copper oxide in slag may also be recovered by this method. The plots of % reduction versus time curves for the carbothermic reduction of slag with carbon black and activated charcoal are shown in figures 4a and 4b, respectively. By comparison, the extent of metallization was higher with activated charcoal (figure 4b) than with carbon black (figure 4a) and this is because, activated charcoal is more reactive than carbon black [25].

The plots of % reduction versus time curves in figures 4a and 4b are characterised by three stages: (i) a slow stage, ≈ 0 % – 7 % reduction, (ii) a very fast or accelerated stage, ≈ 7 – 30 % reduction and, (iii) slightly slower reduction. The slow stage in the first regime shows that the reactivity of carbon black and activated charcoal are both lower [25]. By comparison, the first stage is slower in figure 4a (with carbon black) than in figure 4b (with activated

charcoal) because carbon black is less reactive than activated charcoal [25]. Analysis of the partially reacted samples revealed that metallization of Cu and to a lesser extent Co, occurred in the second regime whereas metallization of Fe occurred mainly in the third regime.

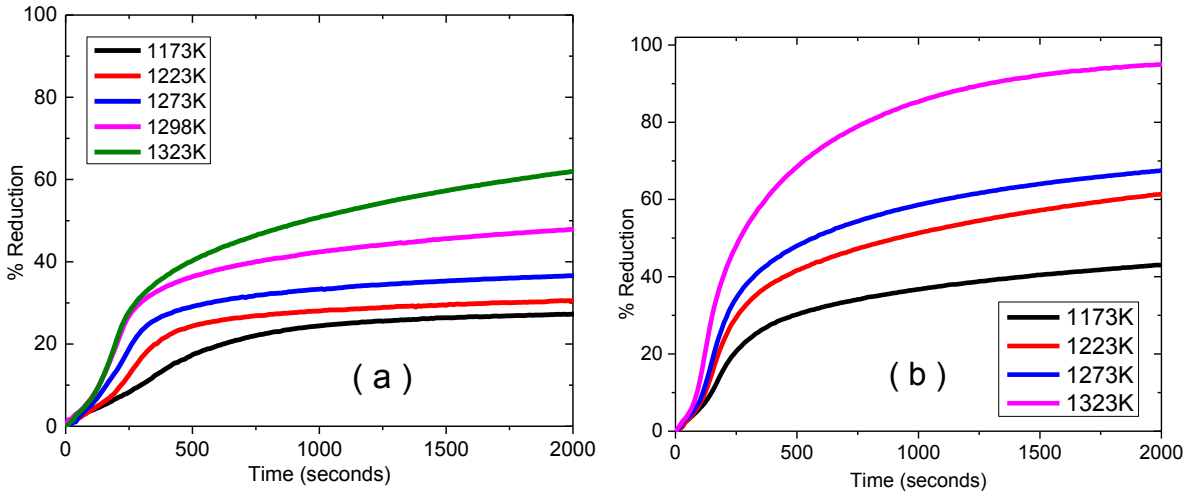

Figure 4 – Carbothermic reduction of slag at molar ratio of MO:C = 1:3; (a) with carbon black and (b) with activated charcoal, argon flow rate = 0.6 litre min^{-1}

The XRD patterns of the samples which were reduced with carbon black and activated charcoal are shown in figures 5a and 5b, respectively. Similar phases are present at 1173 K and 1223 K in figure 5a (with carbon black) and this is in good agreement with the TGA results in figure 4a, as the % reduction only increased by about 4 %R when reduction temperature was increased from 1173 K to 1223 K. It can be observed from figure 5a that metallization of Cu is higher than Co and Fe at 1173 K and this shows that carbon black is less reactive as Cu, Co and Fe are all stable in the presence of reactive carbon above 1173 K [26].

As discussed above, the extent of reduction was higher with activated charcoal (figure 4b) and this is why the XRD peak intensities for Cu and Fe are high in figure 5b. There are no peaks for Co in the XRD patterns in figure 5b because it dissolved in Fe [19, 20].

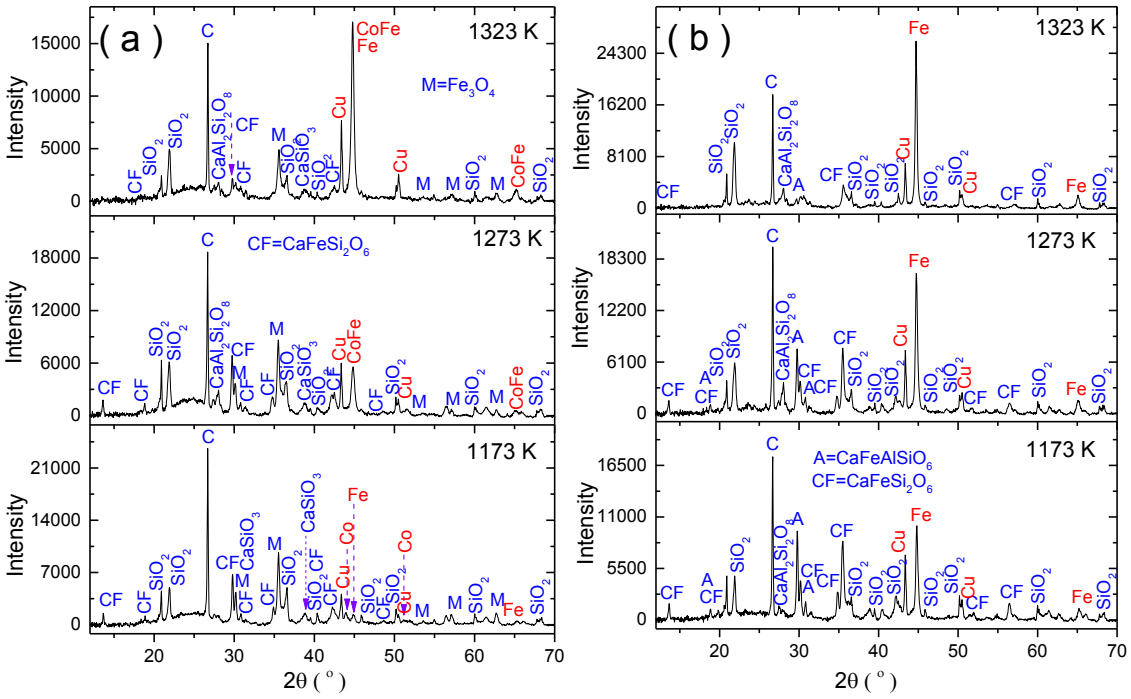

Figure 5 – XRD patterns after reduction of slag at molar ratio of MO:C = 1:3, with; (a) carbon black and (b) activated charcoal. Argon flow rate = 0.6 litre min^{-1}

3.1.1 Reaction mechanism for the carbothermic reduction of slag

As shown from the SEM images in figure 3, the $Co_{0.62}Fe_{2.38}O_4$ crystals are enclosed in the glassy phase and hence carbothermic reduction may occur via diffusion of cations, anions and gases (CO and CO_2 gas) due to lack of contact between metal oxides in slag and solid carbon. The reduction reactions may occur via the following mechanisms:

(i) Diffusion of O^{2-} and metal (M^{2+}) ions from the metal oxide (MO) from the slag to the slag/carbon interface, followed by adsorption of the O^{2-} ions on the carbon surface. The overall rate of reaction may be controlled by the diffusion of O^{2-} and metal (M^{2+}) ions through the slag matrix and/or gasification of carbon.

(ii) Diffusion of carbon or intermediate CO gas through the slag matrix so that the metallic phase is formed within the slag phase.

The SEM images for the samples which were reduced with carbon black and activated charcoal are shown in figures 6a - 6d. The metallic phases are mainly found at the periphery of the particles and partly within the slag phase. The metallic phases at the periphery of the particles were formed via diffusion of the metallic ions (cations) and oxygen ions (anions) from the slag phase. As a result, the overall reactions leading to formation of metallic phase at the periphery

of the slag particle may be represented by equations 10 – 13. The CO gas from equation 11 may diffuse into slag via cracks, to react with the O^{2-} ions (equation 12), causing metallization in the slag phase via equation 12. The diffusion of the CO and CO_2 gases might have occurred through the cracks since the partially reacted samples had several cracks.

$$MO = M^{2+} + O^{2-} \text{ in the slag phase} \quad (10)$$

$$C + O^{2-} = CO(g) + 2e \text{, at slag/carbon interface} \quad (11)$$

$$M^{2+} + 2e = M \text{, at the slag particle periphery or cracks} \quad (12)$$

$$CO(g) + O^{2-} = CO_2(g) + 2e \text{, at the slag particle surface or cracks} \quad (13)$$

The $Co_{0.62}Fe_{2.38}O_4$ crystals [24] are present in the sample after reduction at 1173 K as a result of incomplete reduction. Fe rich slag (≈10 - 13 wt. % Fe) in the form of laths and dendrites and, glassy phase (≈ 3 wt.% Fe) are the other phases at 1173 K.

A significant proportion of Fe is still dissolved in slag at 1323 K, for the reduction with carbon black (figure 6b) as a result of low metallization. The slag in figure 6b has 7 wt.% Fe - 22 wt.% Fe. On the other hand, the fraction of metallic phase is high with activated charcoal at 1323 K (figure 6d) such that slag has less than 5 wt. % Fe. Co and Cu are absent from slag at 1323 K (figures 6b and 6d). In short, only Fe is dissolved in slag at 1323 K and this is due to the fact that: (i) metallization of Fe requires lower partial pressure of O_2 gas than Cu and Co [17, 27] and (ii) the activity of Fe in silicate slag is lower than that of Cu and Co [17].

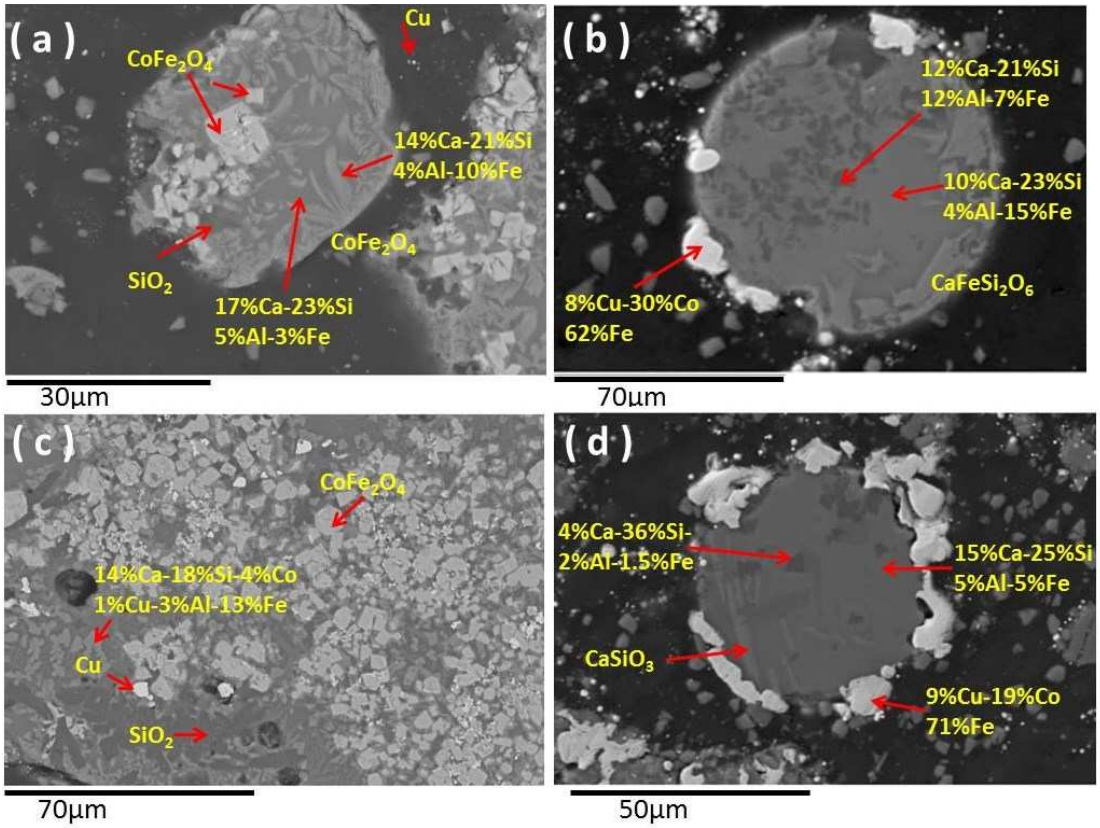

Figure 6 – Backscattered SEM images after reduction of slag at molar ratio of MO:C = 1:3, with: (a) carbon black at 1173 K, (b) carbon black at 1323 K, (c) activated charcoal at 1173 K and (d) activated charcoal at 1323 K

3.3.2 Reaction kinetics for carbothermic reduction of slag

The rate of reduction, derived from the %R versus time plots in figures 4a and 4b, were fitted into the interface model (equation 14) [28], diffusion model (equations 15) [28] and mixed reaction model (equation 16) [29]) in order to establish the reaction mechanism which might be governing the overall rate. The experimental data fitted well with the mixed reaction model in equation 16 as shown in figure 7. Metallization might have been controlled by the mixed reaction model because: (i) the cross-sectional SEM analysis of the reduced samples showed the presence of metallic phases at the periphery of the slag particles (figures 6a - 6d) thereby confirming that there is diffusion of the metallic (M^{2+}) and O^{2-} ions and, (ii) the extent of metallisation was sensitive to reduction temperature and type of carbon, which is a characteristic of a chemically controlled reaction [30].

$$1-(1-X)^{\frac{1}{3}} = Kt \qquad 14$$

$$1-\frac{2}{3}X-(1-X)^{\frac{2}{3}} = Kt \qquad 15$$

$$1-2(1-X)^{\frac{1}{3}}+(1-X)^{\frac{2}{3}} = Kt \qquad 16$$

Where X is the fraction reacted at time t and k is the rate constant

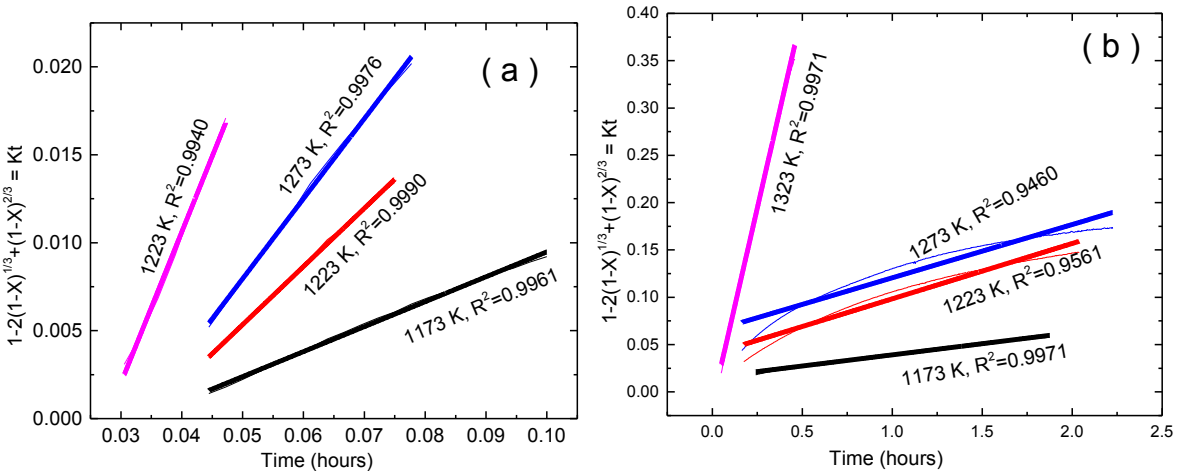

Figure 7 – Plots of $1 - 2(1-X)^{1/3} - (1-X)^{2/3}$ versus time (hours) for the isothermal data at various temperature, with activated charcoal; (a) second regime and (b) third regime

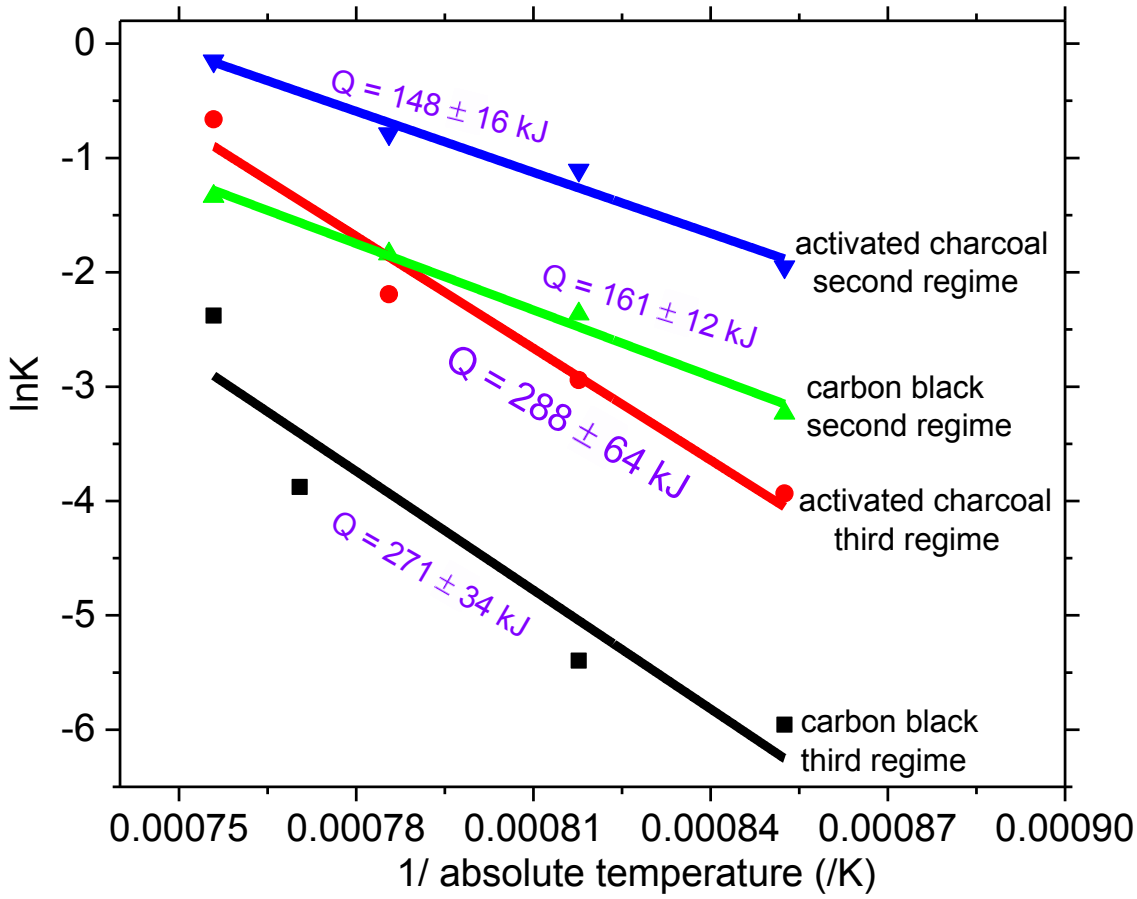

Figure 8 - Arrhenius plots (lnK against reciprocal of temperature) for the carbothermic reduction of slag, the rate constant k was calculated using the G.B + interface model. The activation energy is inserted in each line

The plots of the lnK versus 1/T lines are shown in figure 8 and the calculated value of activation energy are inserted on each fitted line. The activation energy was calculated in the second and third regimes of the % reduction versus time curves (see figures 4a and 4b). The activation energies in the second regime are 161 ± 12 kJ mol^{-1} and 148 ± 14 kJ mol^{-1} with carbon black and activated charcoal, respectively, and they are comparable with the activation energy of 167 kJ for the reduction of Cu from slag [14, 31]. As stated above, metallization of Cu occurred mainly in the second regime. The derived value of activation energies in the third regime are 288 ± 64 kJ mol^{-1} and 271 ± 34 kJ with carbon black and activated charcoal, respectively, and they are comparable with activation energy of: (i) 250 kJ – 350 kJ for the $CO_2(g)$ – C reaction [32-34] and (ii) 300 ± 37 kJ for the diffusion of oxygen in the $Ca_2Al_2SiO_7$ phase in a temperature range of 1273 K – 1573 K [35, 36]. It can be observed in figure 8 that the natural logarithmic values of the rate constant (lnK) are higher for the reduction of slag with activated

charcoal than with carbon black implying that the rate of reductions are higher with the former than with the later.

3.2 Sulphidization of slag in the presence of $CaSO_4$ and graphite

The sulphidization of slag in the presence of $CaSO_4$ was carried out with less reactive carbon (graphite) in order to minimise the formation of CaS [15] via equation 5. The sulphidization of slag in the presence of $CaSO_4$ and graphite was influenced by the reaction temperature and, molar ratio of $CaSO_4$:C.

3.2.1 Effect of molar ratio of graphite

For studying the effect of increasing molar ratio of graphite, the molar ratio of MO:$CaSO_4$ = 1:1.3 and reaction temperature (1323 K) were kept constant and, the XRD results are given in figure 9. The XRD peak intensities for Fe_3O_4 and calcium silicates (Ca_2SiO_4 and Ca_3SiO_5) are very high at molar ratio of MO:$CaSO_4$:C = 1:1.3:0.5 and this shows that: (i) all CaO resulting from the reduction calcination of $CaSO_4$, reacted with SiO_2 and, (ii) part of SO_2 gas from the reduction calcination of $CaSO_4$ escaped out due to insufficient carbon, considering the fact that metal oxides (Cu_2O, CuO, CoO, FeO and Fe_3O_4) cannot be sulphidized with SO_2 gas in the absence of carbon (equation 17).

$$MO + SO_2(g) = MS + 1.5O_2(g) \qquad 17$$

By increasing the molar ratio of graphite to MO:$CaSO_4$:C = 1:1.3:1.5, sulphidization increased and hence the XRD peak intensities for the metal sulphides ($CuFeS_2$, Cu_2S, Cu_5FeS_4) and metal oxide (Fe_3O_4) are high and low, respectively. The higher sulphidization shows that most of the SO_2 gas from the reduction calcination of $CaSO_4$, reacted with the metal oxides to form metal sulphides (see equation 3) at molar ratio of MO:$CaSO_4$:C = 1:1.3:1.5.

Part of Co and Fe were partially reduced to metallic / alloy state (equation 18) when the molar ratio of graphite was increased to MO:$CaSO_4$:C = 1:1.3:2.6. By comparison, metallization of Co and Fe was higher and most of $CaSO_4$ was calcined to CaS (see equation 5) at molar ratio of MO:$CaSO_4$:C = 1:1.3:4. The reduction of $CaSO_4$ to CaS and, high

metallization of Co and Fe resulted in low sulphidization at molar ratio of $MO:CaSO_4:C$ = 1:1.3:4.

$$MO + 0.5\,C(s) = M(s) + 0.5CO_2(g) \qquad 18$$

Turkdogan has recommended that maximum sulphidization may occur at the molar ratio of $CaSO_4:C$ = 1:0.5 [15] but this is not the case based on the results in figure 9 as maximum sulphidization was achieved at the molar ratio of $MO:CaSO_4:C$ = 1:1.3:1.5. It is worth noting that the molar ratio of $CaSO_4:C$ = 1:0.5 is only important for the calcination of SO_2 gas from $CaSO_4$ (equation 2) but extra carbon is needed in the reaction between SO_2 gas and metal oxides (equation 3).

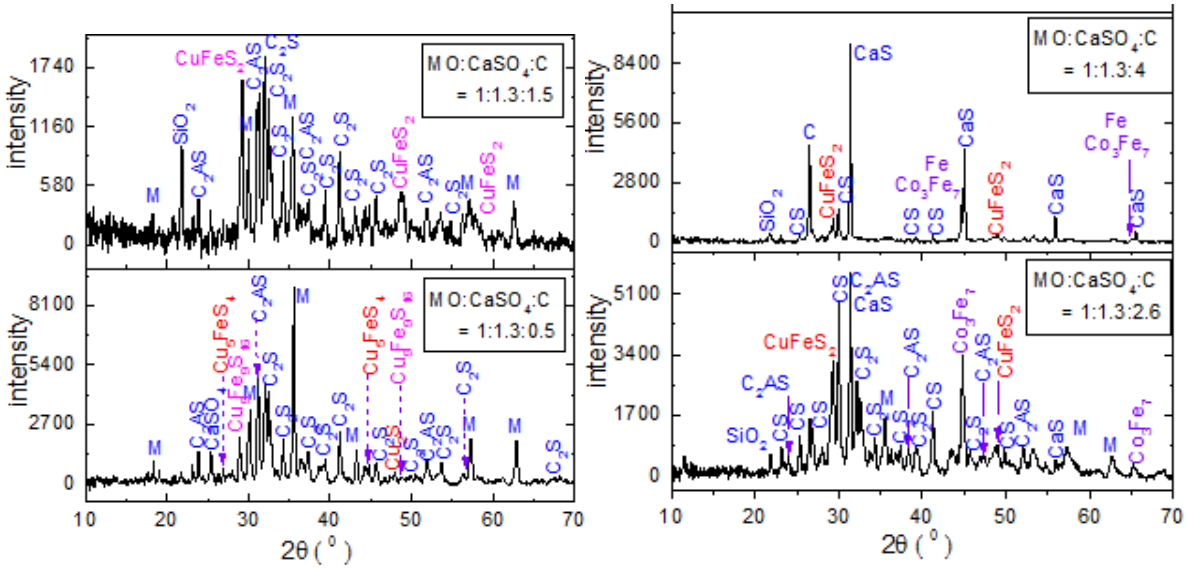

Figure 9 - XRD patterns after sulphidization of slag in the presence of $CaSO_4$ and graphite at 1323 K and different molar ratio of $MO:CaSO_4:C$, M=Fe_3O_4, CS=$CaSiO_3$, C_2S=Ca_2SiO_4 and C_2AS=$Ca_2Al_2SiO_7$

3.2.2 Effect of reaction temperature for sulphidization with graphite

The effect of reaction temperature was studied at the molar ratio of $MO:CaSO_4:C$ = 1:1.3:1.5 and the plots of % conversion versus time curves are shown in figure 10. It can be observed from figure 10 that sulphidization is very sensitive to reaction temperature. For example, the reaction was incomplete after 2 hours at 1173 K but completed within 15 minutes at 1323 K.

The results in figure 10 shows that the extent of conversion is slightly lower at 1323 K than at 1273 K but this may be due to production of CO + CO_2 gases at 1323 K rather than CO_2 gas at T ≤ 1273 K, owing to the increased reactivity of graphite with temperature.

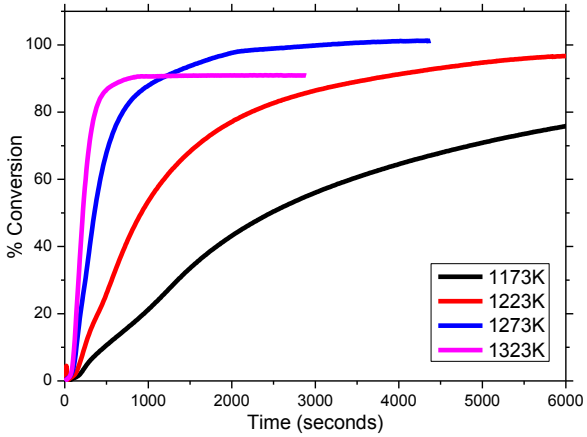

Figure 10 – Plot of conversion versus time curves for the sulphidization of slag in the presence of $CaSO_4$ and graphite, molar ratio of MO:$CaSO_4$:C = 1:1.3:1.5

The XRD patterns of the samples after sulphidizing at various temperatures are shown in figure 11 from which the following observations were made: (i) reduction calcination of $CaSO_4$ was incomplete, after 2 hours at 1173 K and, (ii) part of $CaSO_4$ was calcined to CaS at 1173 K and 1223 K. It is worth noting that the phases obtained at 1173 K and 1223 K agree broadly with the Ca-Fe-O-S system [17] as there is an equilibrium between CaS + Fe_3O_4 and $CaSO_4$ + $Ca_2Fe_2O_5$ phase fields.

The sulphidization of slag in the presence of $CaSO_4$ and carbon can occur, when: (i) sulphur is calcined from $CaSO_4$ and, (ii) metal oxide is reduced to metallic state. Nonetheless, metal oxide cannot be reduced to metallic state when the reactivity of carbon is low and hence sulphidization does not take place. The Gibbs energy change for the reduction of $CaSO_4$ to CaS and that of Fe_3O_4 to Fe are compared in equations 19 and 20, respectively, and it can be observed that equation 19 is more thermodynamically feasible than equation 20. Therefore, equation 20 may occur preferentially, when the reactivity of carbon (graphite) is lower. Based on the thermodynamic prediction in equations 19 and 20 and, the presence of CaS and Fe_3O_4 in the XRD patterns at 1173 K and 1223 K (figure 11), it can be concluded that the sulphidization of Fe in the presence of $CaSO_4$ and graphite was limited by the reduction of

Fe_3O_4. Fe_3O_4 co-exists with $Ca_2Fe_2O_5$ and the formation of the later phase may be represented by equation 21.

$$CaSO_4 + 2C = CaS + 2CO_2(g), \quad \Delta G_{1173\,K} = -244 \text{ kJ} \qquad 19$$

$$Fe_3O_4 + 2C = 3Fe + 2CO_2(g), \quad \Delta G_{1173\,K} = -51 \text{ kJ} \qquad 20$$

$$Fe_3O_4 + 3\,CaSO_4 + \frac{5}{4}C = \frac{3}{2}Ca_2Fe_2O_5 + 3\,SO_2 + \frac{5}{4}CO_2, \qquad 21$$

$$\Delta G_{1173\,K} = -94.5 \text{ kJ}$$

The Gibbs energy change for the carbothermic reduction of FeO, CoO and Cu_2O are compared in equations 22, 23 and 24, respectively, and it can be observed that equation 24 is more thermodynamically feasible and hence preferential metallization of Cu occurred which then led to its sulphidization at 1173 K and 1223 K. The above analysis shows that there is broad agreement between the thermodynamic prediction in equations 22 – 24 and the experimental results at 1173 K and 1223 K (figure 11).

$$2FeO + C = 2Fe + CO_2(g), \quad \Delta G_{1173\,K} = -21 \text{ kJ} \qquad 22$$

$$2CoO + C = 2Co + CO_2(g), \quad \Delta G_{1173\,K} = -93 \text{ kJ} \qquad 23$$

$$2Cu_2O + C = 4Cu + CO_2(g), \quad \Delta G_{1173\,K} = -230 \text{ kJ} \qquad 24$$

The reactivity of graphite increases with increase in temperature such that Fe_3O_4 is reduced to Fe and hence sulphidization of Fe occured above 1223 K.

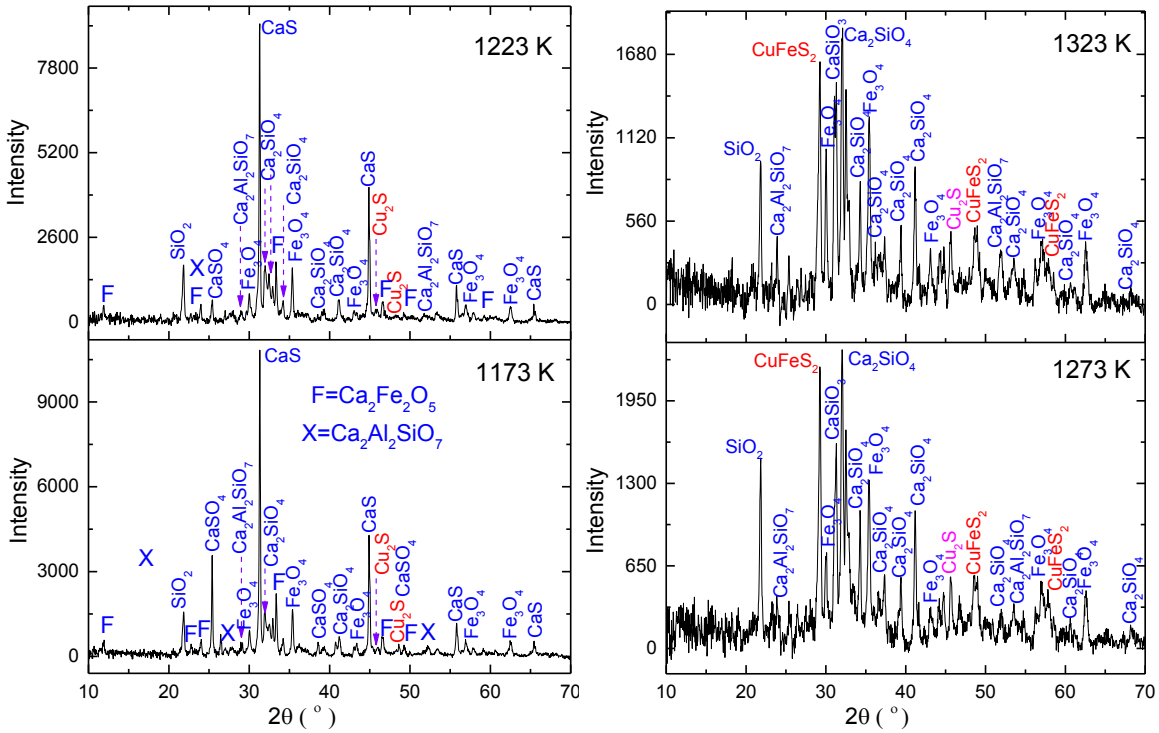

Figure 11 - XRD patterns of the samples, sulphidized in the presence of $CaSO_4$ and graphite, molar ratio of MO:$CaSO_4$:C = 1:1.3:1.5

3.2.4 Estimation of activation energy for sulphidization of slag

The experimental data for the sulphidization of slag in the presence of graphite fit well with the mixed reaction model (equation 16) as shown in figure 12a. The natural logarithmic of the rate constant (gradient for each isothermal in figure 12a) were plotted against the reciprocal of absolute temperature (1/T) for deriving the activation energy and the results are shown in figure 12b. It can be observed from figure 12b that the plot of the lnK versus 1/T line changes at 1273 K and the change in the slope of the line agrees with the XRD results (figure 11) as similar phases were obtained at 1173 K/1223 K and at 1273 K/1323 K. The activation energy is 311 ± 6 kJ in the lower temperature regime (1173 K - 1273 K) is comparable to: (i) activation energy of 305 kJ – 340 kJ for the CO_2 gas – C (graphite) reaction [37-39] in the temperature range of 1123 K – 1373 K and, (ii) enthalpy change of 303 kJ for reaction 25 [27]. Note that the carbothermic reduction of Fe_3O_4 is directly related to the CO_2 – C reaction [40] and hence it can be concluded that the sulphidization reaction was controlled by the reduction of Fe_3O_4 in the lower temperature regime (T < 1273 K).

$$Fe_3O_4 + 2C = 3Fe + 2CO_2(g) \quad 25$$

On the other hand, the activation energy of 215 kJ in the upper temperature regime (T ≥ 1273 K) is comparable to the activation energy of 239 ± 18 kJ, for the reaction between CaS and $CaSO_4$ [41] and this is because, the reduction calcination of $CaSO_4$ to CaO and SO_2 occurs via equations 26 - 28 [15]. The SO_2 gas from equation 28 may react with the metal oxides according to equation 29. The enthalpy change for reaction 28 is 234 kJ $mole^{-1}$ SO_2 gas [15]. By comparing the enthalpy change of 234 kJ and the activation energy of 239 ± 18 kJ for reaction 28 with the activation energy of 215 kJ in the upper temperature regime (figure 12a), it can be concluded that sulphidization of slag in the presence of $CaSO_4$ and graphite, was limited by equation 28.

$$CaSO_4 + C = CaS + 2CO_2(g) \quad 26$$

$$CO_2(g) + C = 2CO(g) \quad 27$$

$$CaS + 3CaSO_4 = 4CaO + 4SO_2(g) \quad 28$$

$$MO + 3CO(g) + SO_2 = MS + 3CO_2(g) \quad 29$$

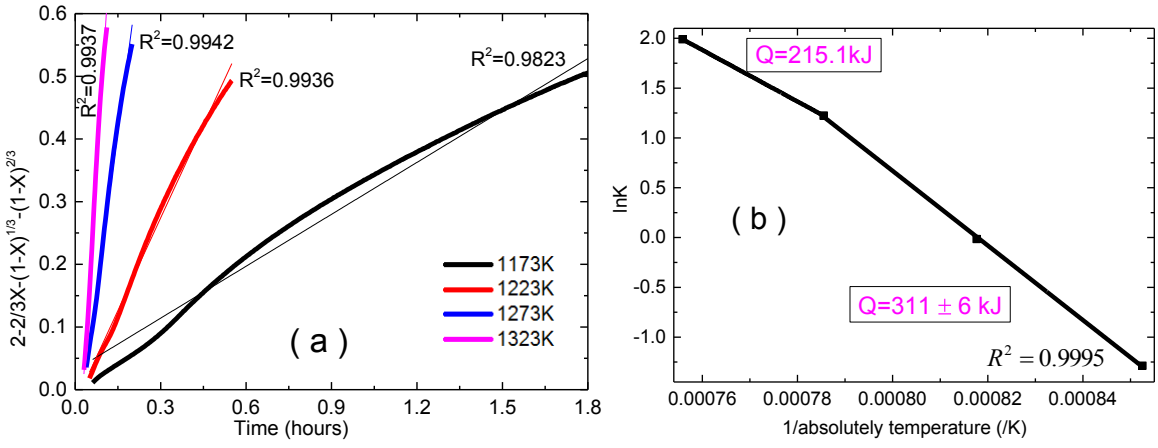

Figure 12 – plots of (a) $2-2/3x-(1-X)^{1/3}-(1-X)^{2/3}$ against time t and (b) lnK against reciprocal of absolute temperature, molar ratio of $MO:CaSO_4:C = 1:1.3:1.3$

3.3 Carbothermic reduction of matte in the presence of CaO

As stated above, copper, cobalt and iron sulphides may be carbothermically reduced to metallic/alloy state in the presence of CaO and hence the sulphidized slag was reacted with CaO and activated charcoal in the temperature range of 1173 K - 1323 K. The plots of % reduction against time curves are shown in figure 13a from which it is apparent that the reduction of sulphidized slag (matte) was much faster than the direct reduction of slag with carbon (MO + C) (see figures 4a and 4b). The reduction of the sulphidized slag was faster due to the presence of liquid phase [42]. The XRD patterns for the reduced sulphidized slag are shown in figure 13b from which the absence of metals sulphides ($CuFeS_2$, Cu_5FeS_4, FeS and Cu_2S) is apparent. Cu, Fe and CoFe were produced as a result of metallization of the sulphidized slag.

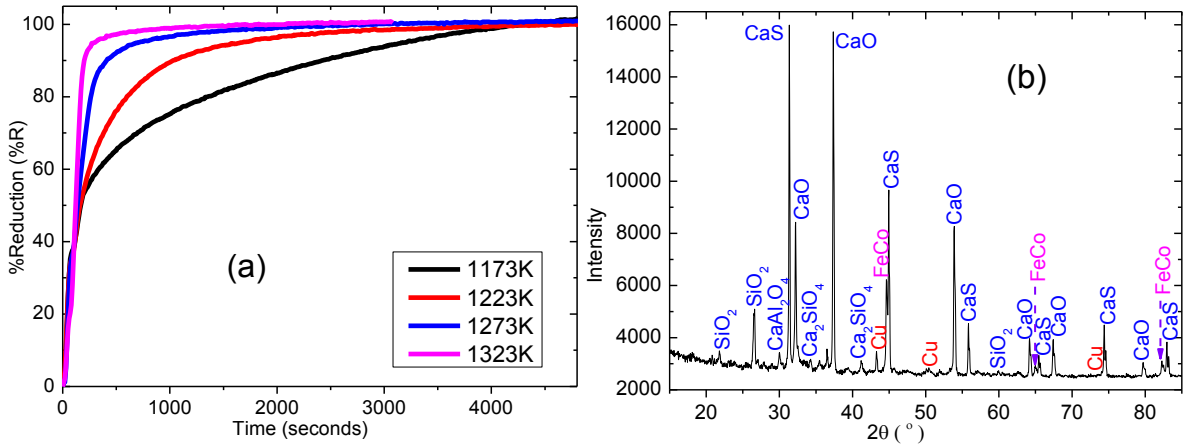

Figure 13 – Carbothermic reduction of sulphidized slag in the presence of CaO with activated charcoal, molar ratio of MS:CaO: C = 1:2:2; (a) TGA results and (b) XRD pattern at 1173K

The backscattered SEM images of the sample that was sulphidized at 1323 K and reduced in the presence of CaO and activated charcoal at 1323 K are presented in figure 14. By comparison, the metallic phases produced via carbothermic reduction of the sulphidized slag are larger than those produced via direct reduction of the slag (see figures 6a and 6d) and this is due to the presence of liquid phases [42].

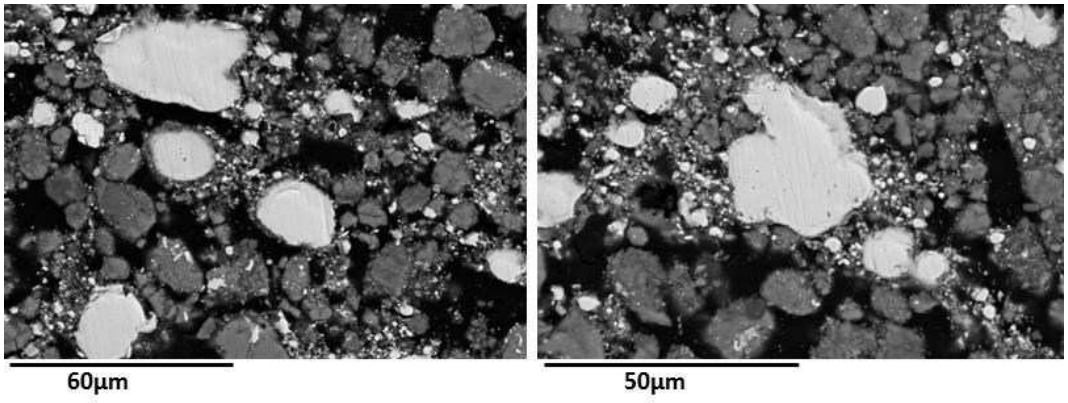

Figure 14 – Backscattered SEM images of the sample, sulphidized at 1323 K and reduced in the presence of CaO and activated charcoal at 1323 K, molar ratio of MS:CaO:C = 1:2:2. The bright particles are the metallic phases

Energy analysis

The theoretical energy requirement for the metallization of Cu, Co and Fe from slag via sulphidization – carbothermic reduction was calculated using HSC 5.1 software [27], based on the following assumptions:

Sulphidization – (i) Cu_2S, CoS and FeS are the only metal sulphides in the sulphidised slag, (ii) alumina is in the form of $CaAl_2Si_2O_8$, (iii) the reactants and products enter and leave the reaction chamber at 298 K and 1323 K, respectively and, (iv) the only product gas is CO_2 gas.

Carbothermic reduction – (i) CO gas is the only gas generated in the reduction of mineral sulphides and (ii) the reactants and products enter and leave the reaction chamber at 1323 K.

The theoretical energy requirement for the sulphidization of slag and carbothermic reduction of the sulphidized slag was calculated as 0.8 kWh and 0.15 kWh, respectively, per kg of slag, giving the total theoretical energy requirement of 0.95 kWh per kg of slag. By comparison, the theoretical energy requirement for smelting slag at 1823 K is 1.1 kWh per kg of slag.

4.0 Conclusions

1. The direct reduction of Cu-Co slag requires higher temperature ($T \geq 1323K$) and a very reactive carbon such as activated charcoal as shown from the % reduction versus time curves in figures 4a and 4b.

2. The activation energies were 288 ± 64 kJ and 271 ± 34 kJ for the carbothermic reduction of slag with carbon black and activated charcoal, respectively, (see figure 8) in the third regime suggesting that the rate determining step is the CO_2 – C reaction, which has the activation energy in the range of 250 kJ – 360 kJ [33, 34].
3. The metal oxides (Cu_2O, CuO, Fe_3O_4, $Co_{0.62}Fe_{2.38}O_4$) were converted into metal sulphides ($CuFeS_2$, Cu_2S, Cu_5FeS_4) via sulphidization of the slag in the presence of $CaSO_4$ as shown in the XRD patterns in figure 11.
4. It is important to control the molar ratio of $CaSO_4$:C. Sulphidization was incomplete at molar ratio of $CaSO_4$:C = 1:0.5 and metallization of Co and Fe occurred at molar ratios of $CaSO_4$:C = 1:2 or 1:4 (see figure 9).
5. Sulphidization of slag in the presence of $CaSO_4$ and graphite was limited by the CO_2 – C(graphite) reaction at T < 1273 K, with an activation energy of 311 ± 6 kJ (see figure 12b).
6. Complete metallization was achieved when the sulphidized slag was reduced in the presence of CaO and activated charcoal (see figures 13a and 13b). The metallic / alloy particles produced via carbothermic reduction of the sulphidized slag were larger (see figure 14) than those produced via direct reduction of the slag with carbon (see figures 6a – 6d).

5.0 Acknowledgement

This paper is a revised version of the paper published in the proceedings on 'Celebrating the Megascale: Proceedings of the Extraction and Processing Division Symposium on Pyrometallurgy in Honor of David G.C. Robertson' edited by Mackey P.J. et. al., published by The Minerals, Metals & Materials Society, Wiley, 2014. The authors gratefully acknowledge the financial support from the Institute of Materials, Minerals and Mining (IOM^3) in London and the Copperbelt University in Zambia.

6.0 References

1. Jones, R.T., et al., *Recovery of cobalt from slag in a DC arc furnace at Chambishi, Zambia.* Journal of The South African Institute of Mining and Metallurgy, 2002. **102**(Compendex): p. 5-9.

2. Davenport, W.G.L., et al., *Extractive Metallurgy of Copper (4th Edition)*. Chemical, Petrochemical & Process. 2002: Elsevier. 1-452.
3. Mututubanya, A., *Cobalt recovery from old Nkana Copper Slag via solid state carbothermic reduction and sulphation*, in *Metallurgy*2013, University of Zambia: Lusaka.
4. Imris, I., *Cobalt distribution in Rokana smelter.* Transactions of the Institution of Mining and Metallurgy, Section C: Mineral Processing and Extractive Metallurgy, 1982. **91**: p. C153-C161.
5. Matusewicz, R. and E. Mounsey, *Using ausmelt technology for the recovery of cobalt from smelter slags.* JOM, 1998. **50**(10): p. 51-52.
6. Tümen, F. and N. Bailey, *Recovery of metal values from copper smelter slags by roasting with pyrite.* Hydrometallurgy, 1990. **25**(3): p. 317-328.
7. Altundoğan, H.S. and F. Tümen, *Metal recovery from copper converter slag by roasting with ferric sulphate.* Hydrometallurgy, 1997. **44**(1–2): p. 261-267.
8. Sukla, L.B., S.C. Panda, and P.K. Jena, *Recovery of cobalt, nickel and copper from converter slag through roasting with ammonium sulphate and sulphuric acid.* Hydrometallurgy, 1986. **16**(2): p. 153-165.
9. Bodsworth, C., *The extraction and refining of metals*. Materials Science and Technology, ed. B. Ralph. 1994, Boca Raton: Fla. : CRC Press. 346.
10. Banda, W., *High Temperature Phase Equilibria in the Fe-Co-Cu-Si system Pertaining to slag cleaning*, in *Department of Process Engineering*2006, Stellenbosch: Stellenbosch.
11. Banda, W., N.T. Beukes, and J.J. Eksteen, *Factors influencing base metal recovery from waste reverberatory furnace slags in a 50 kVA laboratory DC plasma arc furnace.* Journal of The South African Institute of Mining and Metallurgy, 2004. **104**(3): p. 201-207.
12. Jones, R.T. and A.C. Deneys, *Using a direct-current arc furnace to recover cobalt from slags.* JOM, 1998. **50**(10): p. 53-56.
13. Zhai, X.-j., et al., *Recovery of cobalt from converter slag of Chambishi Copper Smelter using reduction smelting process.* Transactions of Nonferrous Metals Society of China, 2011. **21**(9): p. 2117-2121.
14. Reddy, R., V. Prabhu, and D. Mantha, *Recovery of copper from copper blast furnace slag*, in *SME Annual Meeting and Exhibit* 2004: Denver, Colorado.
15. Turkdogan, E.T., *Physical chemistry of high temperature technology* 1980: Academic Press.
16. Mohapatra, B.N.N., Raghvendra; Joshi, S. M.; Cement, . *Effective use of waste generated in thermal power plant as a value added product in cement manufacturing and its environmental impact*. in *International Conference on Waste Technology*. 2010.

17. Bale, C.W., et al., *FactSage thermochemical software and databases.* Calphad: Computer Coupling of Phase Diagrams and Thermochemistry, 2002. **26**(2): p. 189-228.
18. Cutler, C.J., et al. *Phasing out reverbatory furnace operations at KCM Nkana*. in *Southern African Pyrometallurgy 2006*. 2006. Johannesburg.
19. Hara, Y.R.S. and A. Jha. *A Novel Low Energy Route for the Extraction of Copper and Cobalt Metals/Alloys from the Zambian Sulphide Concentrates*. in *Characterization of Minerals, Metals, and Materials*. 2012. John Wiley & Sons.
20. Hara, Y. and A. Jha, *Carbothermic reduction of Zambian sulphide concentrates in presence of lime.* Mineral Processing and Extractive Metallurgy, 2013. **122**(3): p. 146-156.
21. Manasse, A. and M. Mellini, *Chemical and textural characterisation of medieval slags from the Massa Marittima smelting sites (Tuscany, Italy).* Journal of Cultural Heritage, 2002. **3**(3): p. 187-198.
22. Ward, C.R. and D. French, *Determination of glass content and estimation of glass composition in fly ash using quantitative X-ray diffractometry.* Fuel, 2006. **85**(16): p. 2268-2277.
23. Jiménez, J.C.F.-C.G.R.J.M.F., *Occurrence and speciation of copper in slags obtained during the pyrometallurgical processing of chalcopyrite concentrates at the Huelva smelter (Spain).* Journal of Mining and Metallurgy, Section B: Metallurgy 2012. **48**(2): p. 161-171.
24. Ettler, V., et al., *Mineralogy and environmental stability of slags from the Tsumeb smelter, Namibia.* Applied Geochemistry, 2009. **24**(1): p. 1-15.
25. Vignes, A., *Extractive metallurgy 2 Metallurgical reaction processes*. Vol. 2. 2011, London: Wiley.
26. Habashi, F., *Principles of Extractive Metallurgy*. 1969, London: Gordon and Breach. 194 - 196.
27. Roine, A., *HSC Chemistry 5.1*, 2002, Outokumpu Research Oy: Finland.
28. Tathavadkar, V.D., *The process physical chemistry of extraction of sodium chromates from chromite ores*, in *Department of materials school of process, environmental* 2001, Leeds.
29. Ekmekyapar, A., et al., *Investigation of Leaching Kinetics of Copper from Malachite Ore in Ammonium Nitrate Solutions.* Metallurgical and Materials Transactions B, 2012. **43**(4): p. 764-772.
30. Habashi, F., *Kinetics of metallurgical processes*. 1999, Quebec: Metallurgie Extractive.
31. Riveros, G., et al. *Factors Affecting the Rate of Copper Reduction During Copper refining*. in *Yazawa International Symposium, Metallurgical and Materials Processing: Principles and Technologies, Vol. II: High-Temperature Metals Production,*. 2003. Warrendale.
32. Rao, Y.K. and B.P. Jalan, *A study of the rates of carbon-carbon dioxide reaction in the temperature range 839 to 1050 C.* Metallurgical Transactions, 1972. **3**(9): p. 2465-2477.

33. Matsui, I., D. Kunii, and T. Furusawa, *Study of char gasification by carbon dioxide. 1. Kinetic study by thermogravimetric analysis.* Industrial & Engineering Chemistry Research, 1987. **26**(1): p. 91-95.
34. Dutta, S., C.Y. Wen, and R.J. Belt, *Reactivity of Coal and Char. 1. In Carbon Dioxide Atmosphere.* Industrial & Engineering Chemistry Process Design and Development, 1977. **16**(1): p. 20-30.
35. Brady, J.B., *Diffusion Data for Silicate Minerals, Glasses, and Liquids*, in *Mineral Physics & Crystallography: A Handbook of Physical Constants*. 2013, American Geophysical Union. p. 269-290.
36. Yurimoto, H., M. Morioka, and H. Nagasawa, *Diffusion in single crystals of melilite: I. Oxygen.* Geochimica et Cosmochimica Acta, 1989. **53**(9): p. 2387-2394.
37. Turkdogan, E.T., et al., *Rate of oxidation of graphite in carbon dioxide.* Carbon, 1968. **6**(4): p. 467-484.
38. Karata and C., *Catalysis of the graphite–CO2 reaction by iron from in-situ reduction wustite over the range 870–1100°C.* Mineral Processing and Extractive Metallurgy, 2001. **110**(1): p. 7-13.
39. Karatas, C., *Catalytic enhancement of graphite - CO2 reaction by in situ reduced chromium and nickel from their oxides Cr2O3 and NiO over the temperature range 850-1100°C* Mineral Processing and Extractive Metallurgy, 2004. **113**(1): p. 19-24.
40. Rosenqvist, T., *Principles of Extractive Metallurgy (2nd edition)*. 1983, Japan: McGraw.Hill. 460-500.
41. Kutsovskaya, M.L., M.T. Hepworth, and J.R. McGaa, *Recovery of Lime, Sulfur, and Iron from Gypsum and Pyrite Wastes.* Ind. Eng. Chem. Res., 1996. **35**(5): p. 1736-1746.
42. Jha, A., *Carbothermic reduction of sulphide minerals*, in *Department of Metallurgy and Materials Science*1984, Imperial College London.